ELSEVIER

Advances in Water Resources 25 (2002) 1367–1385

Advances in Water Resources

www.elsevier.com/locate/advwatres

Remote sensing in hydrology

Thomas J. Schmugge [a,*], William P. Kustas [a], Jerry C. Ritchie [a], Thomas J. Jackson [a], Al Rango [b]

[a] USDA-ARS Hydrology and Remote Sensing Lab, Beltsville, MD 20705, USA
[b] USDA-ARS Jornada Experimental Range, Las Cruces, NM 88003, USA

Received 11 December 2001; received in revised form 10 May 2002; accepted 11 May 2002

Abstract

Remote sensing provides a means of observing hydrological state variables over large areas. The ones which we will consider in this paper are land surface temperature from thermal infrared data, surface soil moisture from passive microwave data, snow cover using both visible and microwave data, water quality using visible and near-infrared data and estimating landscape surface roughness using lidar. Methods for estimating the hydrometeorlogical fluxes, evapotranspiration and snowmelt runoff, using these state variables are also described.
Published by Elsevier Science Ltd.

1. Introduction

Remote sensing is the process of inferring surface parameters from measurements of the upwelling electromagnetic radiation from the land surface. This radiation is both reflected and emitted by the land. The former is usually the reflected solar while the latter is in both the thermal infrared (TIR) and microwave portions of the spectrum. There is also reflected microwave radiation as in imaging radars. The reflected solar is used in hydrology for snow mapping vegetation/land cover and water quality studies. The thermal emission in the infrared is used for surface temperature and in the microwave for soil moisture and snow studies. We will not discuss the use of radars for precipitation studies as that is the topic of another paper in this issue [50]. We will concentrate on the visible and near-infrared (VNIR) for snow mapping and water quality; the TIR for surface temperature and energy balance studies; passive microwave for soil moisture and snow. Active microwave or radar has promise because of the possibility of high spatial resolution. However, surface roughness effects can make it difficult to extract soil moisture information. Remotely sensed observations can contribute to our knowledge of these quantities and, especially, their spatial variation. With remote sensing we only observe the surface but can obtain the spatial variability and if observations are made repeatedly the temporal variability. In this paper we will concentrate on those applications of remote sensing which we believe are the most promising in hydrology.

A major focus of remote sensing research in hydrology has been to develop approaches for estimating hydrometeorological states and fluxes. The primary set of state variables include land surface temperature, near-surface soil moisture, snow cover/water equivalent, water quality, landscape roughness, land use and vegetation cover. The hydrometeorological fluxes are primarily soil evaporation and plant transpiration or evapotranspiration, and snowmelt runoff.

We will describe methods which have been used to quantify the components of the water and energy balance equation using remote sensing methods. The water balance is commonly expressed as follows:

$$\frac{\Delta S}{\Delta t} = P - ET - Q \tag{1}$$

where $\Delta S/\Delta t$ is the change in storage in the soil and/or snow layer, P is the precipitation, ET is the evapotranspiration and Q is the runoff. Because the energy and water balance at the land surface are closely linked we also need to consider the energy balance equation which is typically written as:

$$R_N - G = H + LE \tag{2}$$

where R_N is the net radiation, G is the soil heat flux, H is the sensible heat flux and LE is the latent heat flux all in

* Corresponding author.
E-mail address: schmugge@hydrolab.arsusda.gov (T.J. Schmugge).

0309-1708/02/$ - see front matter. Published by Elsevier Science Ltd.
PII: S0309-1708(02)00065-9

$W\,m^{-2}$. The quantity $R_N - G$ is commonly referred to as the available energy, and ET and LE represent the same water vapor exchange rate across the surface–atmosphere interface, except ET is usually expressed in terms of depth of water over daily and longer time scales, namely mm/day.

2. Remote sensing of hydrometeorological states

2.1. Land surface temperature

Land surface temperature is the result of the equilibrium thermodynamic state dictated by the energy balance between the atmosphere, surface and subsurface soil and the efficiency by which the surface transmits radiant energy into the atmosphere (surface emissivity). The latter depends on the composition, surface roughness, and physical parameters of the surface, e.g., moisture content. In addition, the emissivity generally will vary with wavelength for natural surfaces. Thus to make a quantitative estimate of the surface temperature we need to separate the effects of temperature and emissivity in the observed radiance. Airborne and satellite-based radiometers measure what is commonly called a 'brightness temperature' derived from the radiance reaching the sensor. This brightness temperature must be corrected for atmospheric attenuation of the surface radiance considering the impact of surface emissivity, before it can regarded as an estimate of the land surface temperature.

The relationship between land surface and brightness temperature from an aircraft or satellite-based sensor is usually expressed in terms of the radiation balance [86],

$$L^j_{SEN} = L^j_{SURF}\tau^j + L^j_{ATM\uparrow} \tag{3}$$

where L is the radiance from the jth waveband channel of the radiometer, L^j_{SEN} is at sensor radiance, L^j_{SURF} is the surface radiance, $L^j_{ATM\uparrow}$ is the upwelling atmospheric radiance and τ^j is the atmospheric transmission. Values of $L^j_{ATM\uparrow}$ and τ^j can be calculated using atmospheric radiative transfer codes, such as MODTRAN [9]. This permits the determination of the upwelling radiance at the surface, which yields the land surface temperature, to be computed from the following expression:

$$L^j_{SURF} = \varepsilon^j L_{BB}(\lambda^j, T_S) + (1-\varepsilon^j)L^j_{ATM\downarrow} \tag{4}$$

where ε^j is the surface emissivity, $L_{BB}(\lambda^j, T_S)$ is the Planck equation for the radiation from a black body and λ^j is the central wavelength for the jth channel of the radiometer. The value of $L^j_{ATM\uparrow}$ can also be determined using atmospheric radiative transfer codes. The remaining problem is to relate these radiances to the surface emissivity without direct knowledge of the land surface temperature, T_{SURF}.

Due to the lack of adequate atmospheric profile observations, the development of alternative approaches such as so-called 'split window' methods would be more operationally applicable (e.g., [87]). These split window methods employ two channels at slightly different wavelengths, λ^1 and λ^2 in Eqs. (4) and (5) to essentially eliminate (using a few approximations) the need for estimating the atmospheric transmission and radiances. This approach has been used quite successfully over oceans where the spectral variation of the emissivity is small. Over land this is not the case and the split window methods are sensitive to uncertainty in the emissivities in the two channels; for example, at a brightness temperature 300 K, a difference $\varepsilon^1 - \varepsilon^2 \sim 0.01$ can yield an error in land surface temperature of $\sim$2 K [87]. There has been much recent work on the use of these split window techniques using the two thermal channels of the advanced very high resolution radiometer (AVHRR) instrument on the NOAA series of meteorological satellites [8,20,48,85,128]. This approach is being used with the multi-spectral TIR data from the moderate resolution imaging spectroradiometer (MODIS) on board the NASA Terra satellite. They use a database of land surface emissivities based on land cover to correct for emissivity effects [129].

Until recently, methods for estimating surface emissivity from remote sensing were empirical. With the launch of NASA's Earth Observing System Platform, Terra, in December 1999, multi-spectral TIR data from the advanced spaceborne thermal emission reflectance radiometer (ASTER; [138]), a technique has been proposed to extract both land surface temperature and emissivity. This approach makes use of a rather robust empirical relation between the range of emissivities and the minimum value from a set of multi-channel observations. It is termed temperature emissivity separation or TES [27]. This algorithm has been evaluated using a prototype of ASTER, the airborne thermal infrared multi-spectral scanner (TIMS), over heterogeneous landscapes in West Africa and in the US southwest [115,117]. In addition, using TIMS data collected in the US Southern Great Plains, the spectral variation of emissivity was used to discriminate between bare soil fields and fields containing senescent vegetation (wheat stubble). Such a separation is not possible with visible and near-infrared data alone and is an important distinction when assessing surface energy balance using remotely sensed temperatures [24].

Land surface temperatures. derived using ASTER satellite imagery covering an area around the USDA-ARS Grazinglands Research Facility in El Reno, Oklahoma is displayed in Fig. 1. The spatial distribution of land surface temperature, T_{SURF}, reflects some significant differences in land cover conditions this time of year (September) with large areas of bare soil and wheat stubble from harvested winter wheat fields and grass-

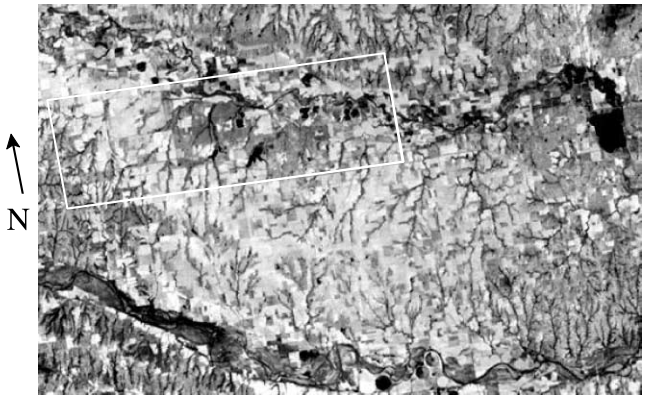

Fig. 1. ASTER TIR imagery for a region in central Oklahoma, just west of Oklahoma City. The data were taken on 4 September 2000 at 17:34 GMT and are for band 13 of ASTER, $\lambda = 10.7$ μm. The temperatures range from 36 °C (black) to 57 °C (white). The spatial resolution is 90 m.

lands used for cattle grazing, with a small areas of irrigated crop lands and water bodies. This type of spatially distributed information is very useful for evaluating spatial patterns of ET over large areas as will be demonstrated later in this paper.

2.2. Near-surface soil moisture

At microwave frequencies the most striking feature of the emission from the earth's surface is large contrast between water and land. This emissivity contrast is due to the large dielectric constant of water (80) while that of most dry minerals or soils is <5, which causes an emissivity contrast of 0.4 for water to about 0.95 for dry land. When you have a mixture of water and dry soil the resulting dielectric constant is between these two extremes thus affording a mechanism for the remote sensing of the moisture content of soils by observing its emissivity at microwave frequencies. Since the early 70s there has been extensive research studying microwave approaches for the remote sensing of soil moisture [42,114,135]. The basic conclusion of this research is that it is indeed possible to determine the moisture content of the surface layer of the soil about a 1/4 of a wavelength thick, i.e., about a 0–5 cm layer using a 21 cm wavelength. In general it has been found that the longer wavelengths are better for increased sampling depth and reduced effects of noise factors such as vegetation and surface roughness. The range of emissivity variation to be expected is from 0.95 for dry soils to less that 0.6 for smooth wet soils. The main factors which affect the accuracy of this determination include: vegetation cover, soil properties, and surface roughness. Vegetation is the most important because a thick enough layer can totally obscure the soil surface from observation. It appears that a mature corn crop (7 kg/m^2) in plant water content is the limiting situation, reducing the sensitivity to about 25% of the bare soil case at the the 21 cm wavelength. Obviously the effect of vegetation would be greater at shorter wavelengths. Thus microwave approaches could not be used to determine soil moisture in many forested situations. The soil properties which effect the microwave response include density and texture, but these factors will change the slope or sensitivity but will not reduce the range of the soil moisture effect. However surface roughness will reduce the range of the microwave response by as much as half in extreme situations, but the more common effect is perhaps a 10% or 20% reduction in sensitivity. Also surface roughness and density are factors which will remain relatively constant due to infrequent working of agricultural fields.

These basic conclusions have been verifed with measurements from field towers, aircraft and to a limited extent satellite platforms. The underlying theory or physical principles and this experimental verification lead us to believe that a 21 cm radiometer of suitable size (20 m) can provide repetitive information about surface soil moisture variations on a global scale with a spatial resolution useful to hydrometeorology and hydroclimatology. In this paper we will provide the documentation for this conclusion along with some results from large scale experiments demonstrating the approach.

Microwave remote sensing offers four unique advantages over other spectral regions:

1. The atmosphere is effectively transparent providing all weather coverage in the decimeter range of wavelengths.
2. Vegetation is semitranparent allowing the observation of underlying surfaces in the decimeter range of wavelengths.
3. The microwave measurement is strongly dependent on the dielectric properties of the target which for soil is a function of the amount of water present.
4. Measurement is independent of solar illumination which allows day or night observation.

Remote sensing cannot replace ground based methods for providing high quality profile data at a point. Its advantage is in mapping conditions at regional, continental and even global scales and possibly on a repetitive basis. Recently it has been shown that repetitive measurements of microwave brightness temperatures can yield subsurface soil hydraulic properties [11].

Passive microwave methods measure the natural thermal emission of the land surface using very sensitive detectors, the intensity of this emission is generally expressed as a brightness temperature, T_B, similar to TIR observations and includes contributions from the atmosphere, reflected sky radiation, and the land surface. However, compared to the TIR wavelengths, atmospheric effects, i.e., atmospheric transmission (τ) and the upwelling radiance ($L^j_{ATM\uparrow}$) in Eq. (3), are negligible at

frequencies below about 6 GHz ($\lambda > 5$ cm). Galactic and cosmic radiation contribute to sky radiation and have a known value that varies very little in the frequency range used for soil water content observations, yielding a $T_{SKY} \sim 4$ K. The brightness temperature of the surface is related to its emissivity, physical temperature and contributions from the intervening atmosphere, yielding an expression similar to Eq. (4)

$$T_B = \varepsilon_M T_M + (1 - \varepsilon_M) T_{SKY} \quad (5)$$

where ε_M and T_M are the emissivity and physical temperature representing some effective depths in the soil surface layer, typically 0–5 cm depth for the emissivity at $\lambda = 21$ cm and a greater depth for the thermal sampling especially for dry soils. Since the second term in Eq. (5) will be on the order of 2 K it is usually neglected thus yielding after rearranging

$$\varepsilon_M = \frac{T_B}{T_M} \quad (6)$$

If T_M is estimated independently, emissivity can be determined. This can be done using surrogates based on satellite surface temperature, air temperature observations, or forecast model predictions. A typical range in ε_M is ~0.9 for a dry soil to ~0.6 for a wet soil comprising the 0–5 cm layer (see below).

As noted earlier, the basic reason microwave remote sensing is capable of providing soil water content information is this large dielectric difference between water and the other soil components. Since the dielectric constant is a volume property, the volumetric fraction of each component must be considered. The computation of the mixture dielectric constant (soil, air and water) has been the subject of several studies and there are different theories as to the exact form of the mixing equation [22,130]. A simple linear weighting function is typically used.

Vegetation reduces the sensitivity of the retrieval algorithm to soil water content changes by attenuating the soil signal and by adding a microwave emission of its own to the microwave measurement. The attenuation increases as frequency increases. This is an important reason for using lower frequencies. At these lower frequencies it is possible to correct for vegetation using a vegetation water content-related parameter. In studies reported in Jackson et al. [44] and Jackson and Schmugge [43], it was found that a linear relationship between the optical depth and vegetation water content, w, could be applied. The vegetation water content can be estimated using a variety of ancillary data sources. One approach is to establish a relationship between w and a satellite based vegetation index such as the normalized difference vegetation index (NDVI) as described in Jackson et al. [47]. Recently multi-angle measurements have used to estimate both vegetation water content and soil moisture [134,136].

The emissivity that results from the vegetation correction is that of the soil surface. This includes the effects of surface roughness. These effects must be removed in order to determine the soil emissivity, which is required in the inversion from microwave brightness temperature to soil moisture. One approach to removing this effect is a model described in Choudhury et al. [18] that yields the bare smooth soil emissivity, with model parameters assigned based upon land use and tillage [46].

The soil moisture sampling depth is the layer of the soil whose dielectric properties determine the surface emissivity and is a function of the microwave frequency or wavelength. There are well known theories describing the reflection resulting from a soil profile with uniform or varying properties [76,137]. The computations involve a nonlinear weighting that decays with depth. Field experiments, suggest that the contributing depth is about 1/4 the wavelength or about 5 cm at $\lambda = 21$ cm [75,132].

There has been a long history (30 years) of aircraft observations of the microwave emission for soil moisture studies [111]. These instruments were non-scanning but generally operated over a range of wavelengths. These early results were instrumental in showing the greater effectiveness of the longer wavelength sensors, the limited sampling depth and the effect of soil texture [112]. An example of these early results is given in Fig. 2 which presents T_B data over a flight line in central South Dakota. The data are for several wavelengths from 1.4 to 21 cm over a range of ground condition, including bare soil, pasture and wheat. The trace of soil moisture is given at the top and it shows that only the pastures had significant levels of moisture and only the 21 cm data showed a response to it. It is from results such as these that we concluded that a radiometer operating at 21 cm would be most effective for soil moisture sensing. To improve the spatial coverage, imaging systems at the 21 cm wavelength were developed. In the late 1980s the 21 cm push broom microwave radiometer was used in several large area mapping experiments, such as FIFE, Monsoon90 and HAPEX-Sahel [113]. During the 1990s, much of this work has used the electronically scanned thinned array radiometer (ESTAR). ESTAR is an L band horizontally polarized instrument that can provide image products. It also is a prototype for a new synthetic aperture antenna technology that is being considered for use in space [62].

For microwave remote sensing of soil moisture to reach its promise it is necessary to develop algorithms to convert the T_B observations to quantitative soil moisture information over large heterogeneous areas on a regular basis. This has been the focus of several recent field experiments. Washita'92 was a large scale study of remote sensing and hydrology conducted by NASA and USDA-ARS using ESTAR over the USDA-ARS Little Washita Watershed facility in southwest Oklahoma [45].

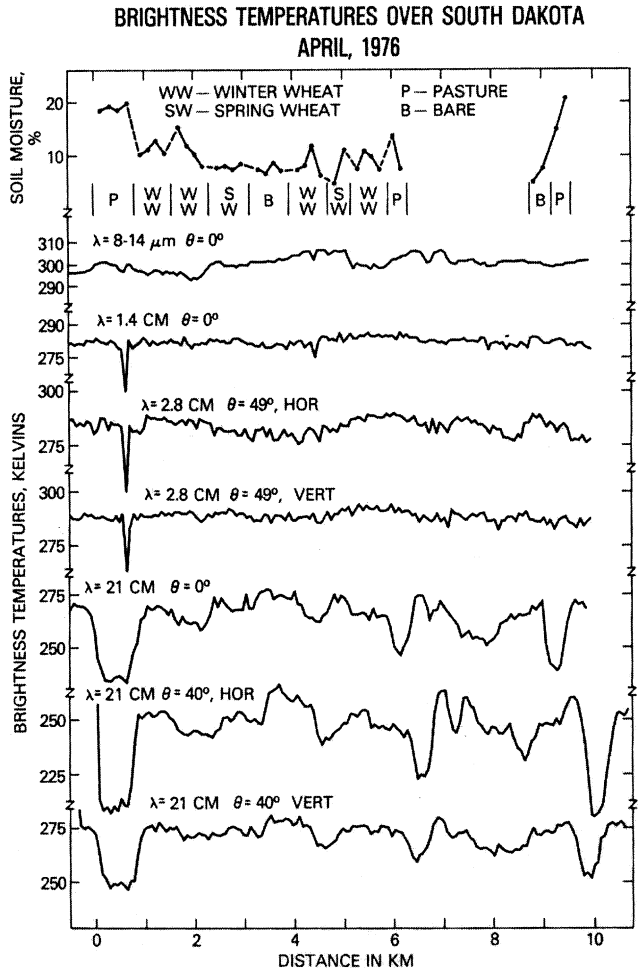

Fig. 2. Brightness temperature traces over a flight line in central South Dakota from April 1976 at several microwave wavelengths. The aircraft altitude was ≈300 m.

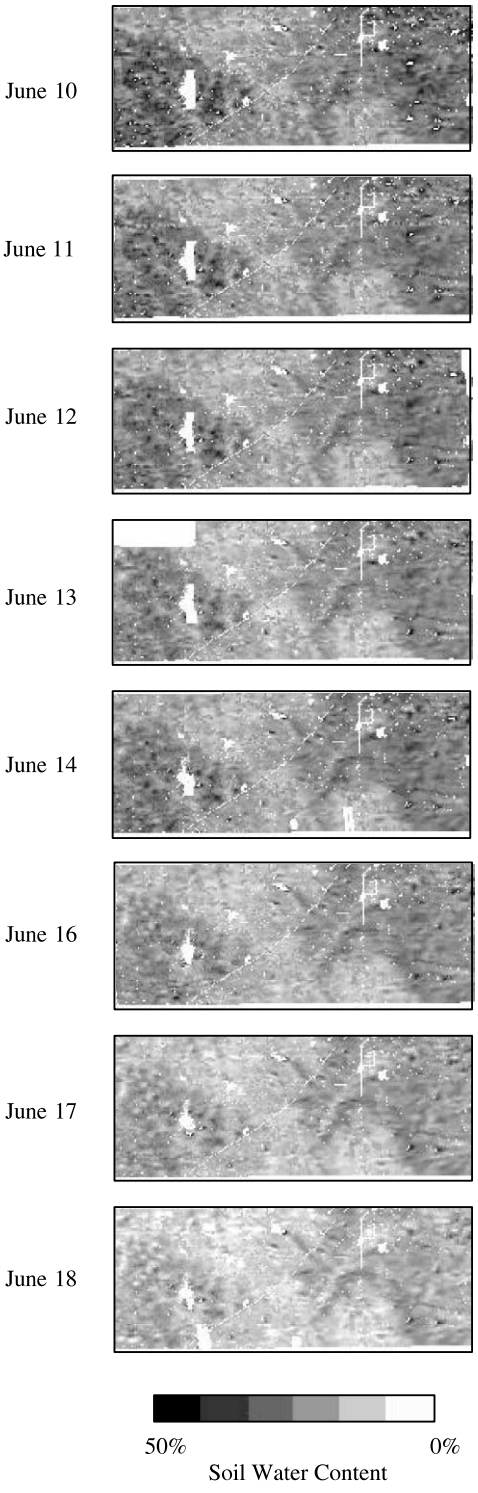

Fig. 3. Near-surface (~0–5 cm) soil water content maps for the USDA-ARS Little Washita Experimental Watershed facility derived from passive microwave data collected on a series of days during Washita'92, June 1992. Spatial resolution is 200 m.

Data collection during the experiment included passive and active microwave observations. Data were collected over a nine day period in June, 1992. The watershed was saturated with a great deal of standing water at the outset of the study. During the experiment there was no rainfall and surface soil water content observations exhibited a drydown pattern over the period. Surface soil water content observations were made at sites distributed over the area. Significant variations in the level and rate of change in surface soil water content were noted over areas dominated by different soil textures.

Passive microwave observations were made on eight days. The ESTAR data were processed to produce brightness temperature maps of a 740 km^2 area on each of the eight days. Using the algorithm developed by Jackson et al. [45], these data were converted to soil water content images. Gray scale images for each day are shown in Fig. 3. These data exhibited significant spatial and temporal patterns. Spatial patterns were clearly associated with soil textures and temporal patterns with drainage and evaporative processes. Relationships between the ground sampled soil water content and the brightness temperatures were consistent with previous results. These data have also been used by

Rodriguez-Iturbe et al. [108] to study the statistical structure of soil moisture fields. They did this by aggregating the pixels up to a 1 km × 1 km size and looking at the variance in the data as a function of pixel area. They found a power law relationship between the variance and pixel area with the variance decreasing as the area increased. The slope of the relationship changed, generally increasing, as the soils dried.

More recently, ESTAR collected data over a much larger domain, mapping an area (~40 km east–west and ~260 km north–south) as part of the 1997 Southern Great Plains Experiment (SGP97; [47]). The area mapped encompassed the USDA-ARS Little Washita Watershed, USDA-ARS Grazinglands Research Facility and Department of Energy Atmospheric Radiation Measurement, Cloud and Radiation Test Bed, Central Facility. SGP97 was designed and conducted to extend surface soil moisture retrieval algorithms based on passive microwave observations to coarser resolutions, larger regions with more diverse conditions, and longer time periods. The ESTAR instrument was used for daily mapping of surface soil moisture over a one month period from mid-June to mid-July. Results showed that the soil moisture retrieval algorithm performed the same as in previous investigations (e.g., Washita'92), demonstrating consistency of both the retrieval and the instrument.

Satellite based sensors offer the advantages of large area mapping and long-term repetitive coverage. For most satellite systems the revisit time can be a critical problem in studies involving rapidly changing conditions such as surface soil water content. With very wide swaths it is possible to obtain twice daily coverage with a polar orbiting satellite. For most satellites, especially if constant viewing angle is important, the revisit time can be much longer. Optimizing the time and frequency of coverage is a critical problem for soil water content studies. Currently, all passive microwave sensors on satellite platforms operate at high frequencies (>7 GHz). A more recent option is the multiple frequency advanced microwave scanning radiometer (AMSR) satellite systems that will include a 6.9 GHz channel. AMSR holds great promise for estimating soil water content in regions of low levels of vegetation. AMSR is not the optimal solution to mapping soil water content but it is the best possibility in the near term. Based on the published results and supporting theory [1,17,77,82,131], this instrument should be able to provide surface moisture information in regions of low vegetation cover, $<1\ \mathrm{kg\,m^{-2}}$ vegetation water content. To pursue the use of space observations further research programs are underway to develop a space based system with a 1.4 GHz channel which would provide improved global soil moisture information [49]. The soil moisture and ocean salinity mission is currently being implemented by the European Space Agency. This instrument will extend the aperture synthesis approach pioneered by ESTAR to two dimension and will make dual polarized measurements at a range of angles. With these data it is expected to be able obtain not only soil moisture but also vegetation water content at a 50 km resolution [136].

2.3. Snow cover and water equivalent

The occurrence of precipitation in the form of snow as opposed to rain typically causes a change in how a drainage basin responds to the input of water. The reason for the modified hydrological response is that snow is held in cold storage on a basin for an extended period of time before it enters the runoff process. There is such a vast difference in the physical properties of snow and other natural surfaces that the occurrence of snow on a drainage basin can cause significant changes in the energy and water budgets. As an example, the relatively high albedo of snow reflects a much higher percentage of incoming solar shortwave radiation than snow-free surfaces (80% for relatively new snow as opposed to roughly 15% for snow-free vegetation). Snow may cover up to 53% of the land surface in the northern hemisphere [23] and up to 44% of the world's land areas at any one time. Snow cover and the equivalent amount of water volume stored supplies at least one-third of the water that is used for irrigation and the growth of crops worldwide [121]. In high mountain snowmelt basins of the Rocky Mountains, USA, as much as 75% of the total annual precipitation is in the form of snow [123], and 90% of the annual runoff is from snowmelt [34].

Snow cover can be detected and monitored with a variety of remote sensing devices. The greatest number of applications have been found in the VNIR region of the electromagnetic spectrum. Because of Landsat and SPOT frequency of observation problems, many users have turned to the NOAA polar orbiting satellite with the AVHRR, which has a resolution of about 1 km in the 0.58–0.68 μm red band. The frequency of coverage is twice every 24 h (one daytime pass and one nighttime pass). The major problem with the NOAA-AVHRR data is that the resolution of 1 km may be insufficient for snow mapping on small basins. Data from the MODIS instrument on NASA's EOS satellites with 250 m resolution in two visible bands will partially alleviate this problem.

Despite the various problems mentioned, visible aircraft and satellite imagery have been found to be very useful for monitoring both the buildup of snow cover in a drainage basin and, even more importantly, the disappearance of the snow covered area in the spring. This disappearance or depletion of the snow cover is important to monitor for snowmelt runoff forecasting purposes. It has been recommended that the optimum frequency of observation of the snow cover during de-

pletion would be once a week [91]. Depending on the remote sensing data used, it could be very difficult to obtain this frequency. Certain snowmelt runoff applications have been possible with as few as two to three observations during the entire snowmelt season [91].

Snow on the earth's surface is, in simple terms, an accumulation of ice crystals or grains, resulting in a snowpack which over an area may cover the ground either completely or partly. The physical characteristics of the snowpack determine its microwave properties; microwave radiation emitted from the underlying ground is scattered in many different directions by the snow grains within the snow layer, resulting in a microwave emission at the top of the snow surface being less than the ground emission. Properties affecting microwave response from a snowpack include: depth and water equivalent, liquid water content, density, grain size and shape, temperature and stratification as well as snow state and land cover. The sensitivity of the microwave radiation to a snow layer on the ground makes it possible to monitor snow cover using passive microwave remote sensing techniques to derive information on snow extent, snow depth, snow water equivalent (SWE) and snow state (wet/dry). Because the number of scatterers within a snowpack is proportional to the thickness and density, SWE can be related to the brightness temperature of the observed scene [39]; deeper snowpacks generally result in lower brightness temperatures.

The general approach used to derive SWE and snow depth from passive microwave satellite data relates back to those presented by Rango et al. [90] and Kunzi et al. [51] using empirical approaches and Chang et al. [16] using a theoretical basis from radiative transfer calculations to estimate snow depth from SMMR data. As discussed in Rott [109], the most generally applied algorithms for deriving depth or SWE are based on the generalized relation given in Eq. (6)

$$SWE = A + B\frac{T_B(f_1) - T_B(f_2)}{f_2 - f_1} \tag{7}$$

in mm, for $SWE > 0$, where A and B are the offset and slope of the regression of the brightness temperature difference between a high scattering channel (f_2, commonly 37 GHz) and a low scattering one (f_1, commonly 18 or 19 GHz) of vertical or horizontal polarization. No single global algorithm will estimate snow depth or water equivalent under all snowpack and land cover conditions. The coefficients are generally determined for different climate and land covered regions and for different snow cover conditions; algorithms used in regions other than for which they were developed and tested usually provide inaccurate estimates of snow cover. Also, accurate retrieval of information on snow extent, depth, and water equivalent requires dry snow conditions, because the presence of liquid water within the snowpack drastically alters the emissivity of the snow, resulting in brightness temperatures significantly higher than if that snowpack were dry. Therefore, an early morning overpass (local time) is the preferred orbit for retrieval of snow cover information to minimize wet snow conditions. It is also recognized that knowledge of snowpack state is useful for hydrological applications. Regular monitoring allows detection of the onset of melt or wet snow conditions [36].

Passive microwave data provides several advantages not offered by other satellite sensors. Studies have shown that passive microwave data offer the potential to extract meaningful snowcover information, such as SWE, depth, extent and snow state. SSM/I is a part of an operational satellite system, providing daily coverage of most snow areas, with multiple passes at high latitudes, hence allowing the study of diurnal variability. The technique has generally all-weather capability (although affected by precipitation at 85 GHz), and can provide data during darkness. The data are available in near-real time, and hence can be used for hydrological forecasting. There are limitations and challenges in using microwave data for deriving snow cover information for hydrology. The coarse resolution of passive microwave satellite sensors such as SMMR and SSM/I ($\sim$25 km) is more suited to regional and large basin studies, although Rango et al. [93] did find that reasonable SWE estimates could be made for basins of less than 10,000 km^2. The AMSR launched on NASA's EOS satellite, AQUA, 4 May 2002 will provide a wider range of wavelengths and with better spatial resolution than what is currently available.

Another challenge is to incorporate the effect of changing snowpack conditions throughout the winter season. Seasonal aging, or metamorphism, results in a change in the grain size and shape, and this will affect the microwave emission from the snowpack. In very cold regions, depth hoar characterized by its large crystal structure enhance the scattering effect on the microwave radiation, resulting in lower surface emission producing an overestimate of SWE or snow depth [5,38]. The increase in brightness temperature associated with wet snow conditions currently prevents the quantitative determination of depth or water equivalent since algorithms will tend to produce zero values under these conditions. The best way to view the seasonal variability in microwave emission from the snowpack is to compile a time series of satellite data spanning the entire season which can then be related to changes in the pack over the season [127].

In Canada, a federal government program (Climate Research Branch, Atmospheric Environment Service) has been ongoing since the early 1980s to develop, validate and apply passive microwave satellite data to determine snow extent, SWE and snowpack state (wet/dry) in Canadian regions for near-real time and operational

use in hydrological and climatological applications. Goodison and Walker [36] provide a summary of the program, its algorithm research and development, and future thrusts. For the prairie region a SWE algorithm was empirically derived using airborne microwave radiometer data [37], and tested and validated using Nimbus-7 SMMR and DMSP SSM/I satellite data [35]. After 10 winter seasons in operation, the Canadian prairie SWE mapping program has successfully demonstrated a useful application of SSM/I derived snow cover information for operational hydrological analyses. It is also a cooperative program in that user feedback has served to enhance the validation and the refinement of the SSM/I SWE algorithm [36]. One enhancement has been the development of a wet snow indicator [126], which overcomes a major limitation of the passive microwave technique by providing the capability to discriminate wet snow areas from snow-free areas and hence a more accurate retrieval of snow extent during melting conditions.

Because areal snow cover extent data have been available since the 1960s, various investigators have found many useful applications. A team of scientists from a variety of US government agencies developed plans in the early 1980s for operational snow mapping by the US National Weather Service (NWS) for hydrological purposes. In 1986, NWS adopted these plans and proceeded to develop operational remote sensing products, mostly for snow hydrology. The most widely distributed products of the NWS National Operational Hydrologic Remote Sensing Center are periodic river basin snow cover extent maps from NOAA-AVHRR and the geostationary operational environmental satellite (GOES). Digital maps for about 4000 basins in North America are produced about once per week and are used by a large group of users including the NWS River Forecast Centers and individual water authorities.

Very few hydrological models have been developed to be compatible with remote sensing data. One of the few models that was developed requiring direct remote sensing input is the snowmelt runoff model (SRM) [64]. SRM requires remote sensing measurements of the snow covered area in a basin. Although aircraft observations can be used, satellite-derived snow cover extent is the most common. SRM employs the degree day approach to melting the snow cover in a basin. To date, this version of SRM has been successfully tested on over 80 basins in 25 countries worldwide.

Spain is also using NOAA-AVHRR snow cover data for the forecasting of snowmelt runoff volume during the spring and summer months in the Pyrenees. Development of subpixel analysis techniques [31] has allowed snow cover mapping on basins as small as 10 km^2 using the AVHRR data. This approach could make NOAA-AVHRR data more widely useable for hydrological applications after it is tested in different geographic regions. Gomez-Landesa and Rango [32] applied NOAA-AVHRR snow cover data as input to the SRM for use in forecasting the seasonal snowmelt runoff volume in the Pyrenees to assist in planning hydropower production. More recently, Gomez-Landesa and Rango [33] compared snow cover mapping of NOAA-AVHRR

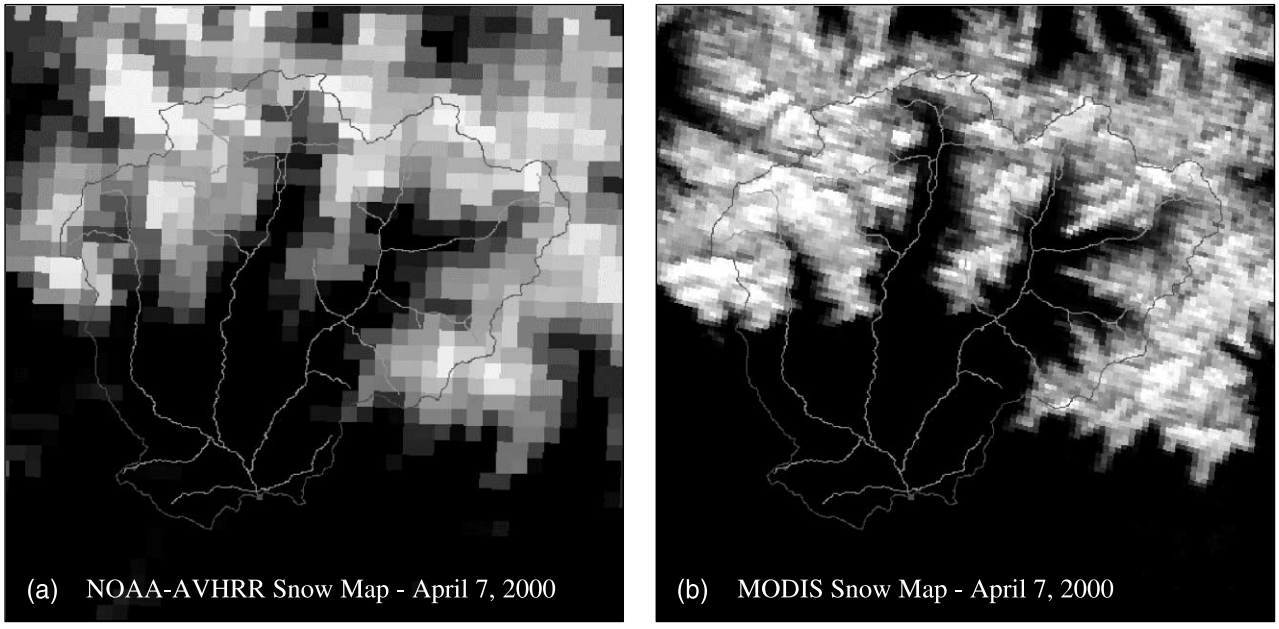

Fig. 4. NOAA-AVHRR (a) and MODIS (b) derived snow cover derived snow cover for the Noguera Ribagorzana Basin (572.9 km^2) in the Central Pyrenees of Spain on 7 April 2000. The different gray levels correspond to different percents of snow cover in each NOAA-AVHRR and MODIS pixel.

with the higher resolution (250 m pixel) data from the MODIS on NASA's Terra satellite platform. Fig. 4 shows the NOAA-AVHRR and MODIS derived snow cover for the Noguera Ribagorzana Basin (572.9 km^2) in the Central Pyrenees of Spain on 7 April 2000. The different gray levels correspond to different percents of snow cover in each NOAA-AVHRR and MODIS pixel. The correlation between AVHRR and MODIS snow maps were on the order of 0.8–0.9 with good agreement between the snow distribution with altitude obtained from both instruments. The agreement was good even in very small basins with an area ~8.3 km^2.

2.4. Landscape roughness and vegetation cover

Roughness refers to the unevenness of the earth's surface due to natural processes (i.e., topography, vegetation, erosion) or human activities (i.e., buildings, power lines, forest clearings). Roughness affects transport of hydrometeorological fluxes between the land surface and atmosphere as well as below the surface, i.e., infiltration and water movement. Roughness is often separated in different complexities related to its effects on land surface–atmosphere dynamics. The complexities are (1) vegetation and urban roughness where the horizontal scale is relatively small, (2) transition roughness between landscape patches (i.e., plowed field next to a forest), and (3) topographic roughness due to changing landscape elevations. These complexities and scales have different effects on wind, heat, and water movement and are difficult to measure in the field at large scales. Lidar, synthetic aperture radar (SAR), digital elevation models, and photogrammetry are among the remote sensing techniques that have been used to measure landscape surface roughness properties over large areas.

The need for accurate and rapid measurements and assessments of land surface terrain features to estimate the effects of land surface roughness on hydrometeorological processes led to the application of lidar distancing technology from an aircraft-based platform [94,98]. Satellite platforms have also been employed [40].

The first applications of the airborne lidar altimeter were to measure topography [63] and sea ice roughness [106]. Lidar altimeters can measure long topographic profiles quickly and efficiently. An example of a topographic profile is shown in Fig. 5 using ≈45 s of profiling lidar altimeter data collected in the USDA-ARS Reynolds Creek Experimental Watershed. The length of this profile is 3.5 km and was part of a 10 km profile. The inset in Fig. 5 shows the data at full resolution making the vegetation canopy visible in greater detail. Topographic, transitional, and canopy roughness can be determined from this profile. Ease and speed of data collection would allow measurement of several profiles with a minimum of extra survey cost. Rango et al. [92] used scanning lidar data to study morphological characteristics of shrub coppice dunes in the USDA-ARS Jornada Experimental Range situated within the Chihuahuan desert. They calculated dune distribution, area, and volume from the scanning laser data. Lidar measurements provide spatial data necessary to understand the effects of topography at all scales on roughness patterns of the landscape.

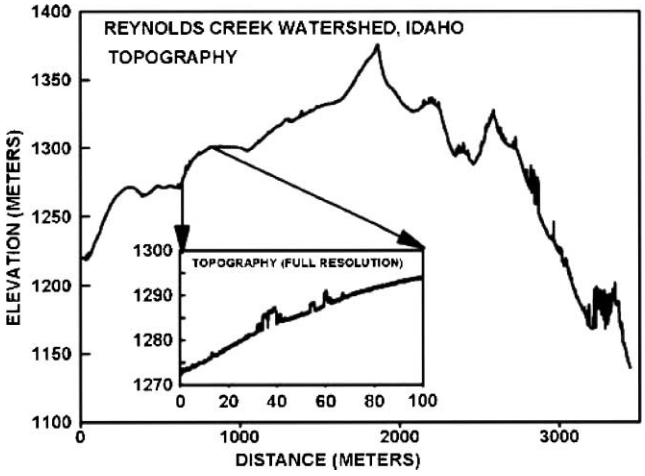

Fig. 5. A topographic profile measured using an airborne lidar altimeter. The profile was made by block averaging 16 lidar measurements. The insert shows a 100 m section at full resolution (no averaging).

Detailed measurements of microtopography over distances of 1–2 m to understand the development and patterns of surface roughness using a profiling airborne lidar altimeter for a bare agricultural field is shown in Fig. 6 (upper profile). This profile shows the surface microroughness superimposed on the overall topography measured with a lidar altimeter. A moving average filter was used to remove random and system noise [65] and is shown with the lower profile in Fig. 6. Microroughness of soil and vegetation has been shown to influence rill development, germination, water retention,

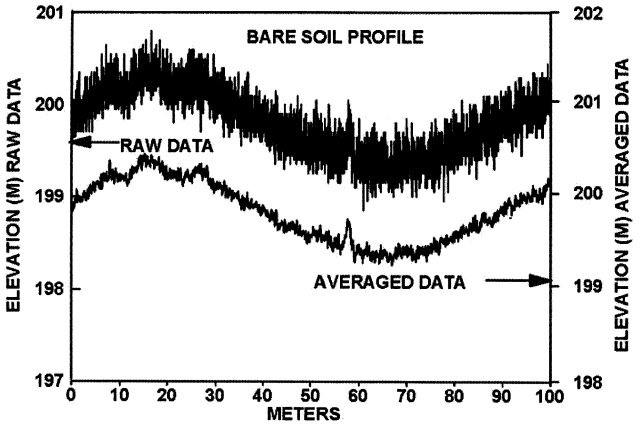

Fig. 6. A bare soil profile measured in an agricultural field. The lower profile was derived from the upper profile (raw data) using a 1 1 measurement moving average filter.

infiltration, evaporation, runoff, and soil erosion by water and wind [139]. Lidar altimeter measurements of microroughness of the landscape surface can be used to understand and calculate the effects of roughness on evaporation, soil moisture, runoff, and soil erosion at field and landscape scales.

Entrenched erosional features need to be quantified to estimate their effects on water movement and soil loss across the landscape. Measurements of these features can be difficult and time consuming using ground-based techniques. Measurement of large erosional landscape features can be made rapidly using airborne lidar data [97]. The shape and roughness of gullies and stream channels can be defined (see Fig. 7). The lower dotted line in figure represents the maximum stage of this stream channel cross section, but other stages could be represented and used to calculate the carrying capacity at different channel and floodplain stages. Data on stream bottom roughness can also be used to estimate resistance to flow of the stream. Channel and flood plain cross sections and roughness allow better estimates of channel and flood plain carrying capacity and resistance to flow. Data on channel, gully, and flood plain size, roughness, and degradation can help in design, development, and placement of physical structures to control and calculate flows.

Vegetation canopies are an important part landscape roughness that are difficult to measure by conventional techniques. Airborne lidar measurements provided accurate measurements of canopy top roughness (Fig. 8a), heights (Fig. 8b) and cover [95,96,133]. Scanning lasers [92] can provide a 3D view of canopy structure needed understand canopy roughness. Lidar measurements of vegetation properties were made at eight locations in the USDA-ARS Walnut Gulch Experimental Watershed in Arizona [133] and used in an algorithm for estimating

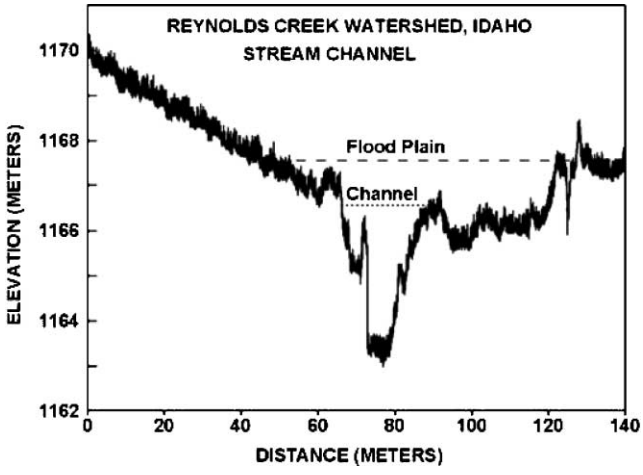

Fig. 7. A lidar altimeter measured stream cross section. Lower dashed line represents the stream cross section and upper dashed line represents the flood plain cross section.

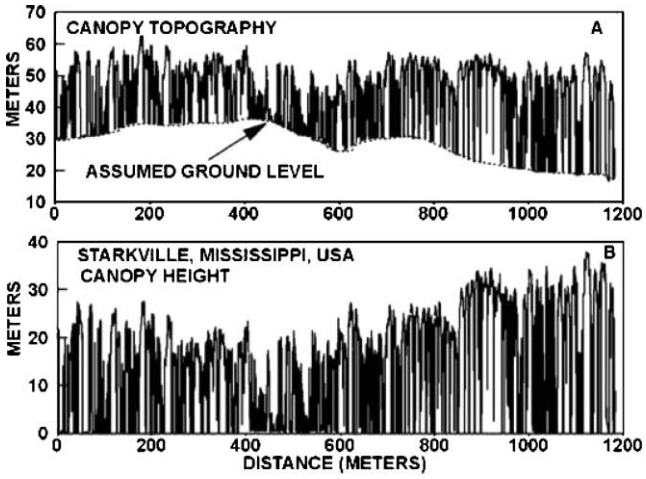

Fig. 8. A forest canopy (a) and tree heights (b) measured using an airborne lidar altimeter.

effective aerodynamic roughness, an important parameter in ET models [68]. These remote estimates agreed with aerodynamic roughness calculated from micrometeorological methods using tower-based measurements [52]. Fractals calculated for lidar data have also been used as a way to separate roughness [83,84,99] due to topography and vegetation and to show seasonal patterns in roughness. This type of information from lidar should provide more accurate parameter estimation for models computing hydrometeorological fluxes.

2.5. Remote sensing techniques to assess water quality

Water quality is a general descriptor of water properties in terms of physical, chemical, thermal, and/or biological characteristics. In situ measurements and collection of water samples for subsequent laboratory analyses provide accurate measurements for a point in time and space but do not give either the spatial or temporal view of water quality needed for accurate assessment or management of water bodies. Substances in surface water can significantly change the backscattering characteristics of surface water. Remote sensing techniques for monitoring water quality depend on the ability to measure these changes in the spectral signature backscattered from water and relate these measured changes by empirical or analytical models to water quality parameters. The optimal wavelength used to measure a water quality parameter is dependent on the substance being measured, its concentration, and the sensor characteristics.

Major factors affecting water quality in water bodies across the landscape are suspended sediments (turbidity), algae (i.e., chlorophylls, carotenoids), chemicals (i.e., nutrients, pesticides, metals), dissolved organic matter (DOM), thermal releases, aquatic vascular plants, pathogens, and oils. Suspended sediments, algae,

DOM, oils, aquatic vascular plants, and thermal releases change the energy spectra of reflected solar and/or emitting thermal radiation from surface waters which can measured by remote sensing techniques. Most chemicals and pathogens do not directly affect or change the spectral or thermal properties of surface waters so they can only be inferred indirectly from measurements of other water quality parameters affected by these chemicals.

Empirical or analytical relationships between spectral properties and water quality parameters are established. The general forms of these empirical equations are

$$Y = A + BX \quad \text{or} \quad Y = AB^X \tag{8}$$

where Y is the remote sensing measurement (i.e., radiance, reflectance, energy) and X is the water quality parameter of interest (i.e., suspended sediment, chlorophyll). A and B are empirically derived factors. In empirical approaches statistical relationships are determined between measured spectral/thermal properties and measured water quality parameters. Often information about the spectral/optical characteristic of the water quality parameter is used to aid in the selection of best wavelength(s) or best model in this empirical approach. The empirical characteristics of these relationships limit their applications to the condition for which the data were collected.

Suspended sediments are the most common pollutant both in weight and volume in surface waters of freshwater systems [61,107]. Suspended sediments increase the radiance emergent from surface waters (Fig. 9) in the VNIR proportion of the electromagnetic spectrum [105]. Significant relationships between suspended sediments and radiance or reflectance from spectral wavebands or combinations of wavebands on satellite and aircraft sensors have been shown. Curran and Novo [19] in a review of remote sensing of suspended sediments found that the optimum wavelength was related to suspended sediment concentration. Ritchie and Cooper [101,102] showed that an algorithm for relating remotely sensed data to the sediment load developed for one year was applicable for several years. Once developed, an algorithm should be applicable until some watershed event changes the quality (size, color, mineralogy, etc.) of suspended sediments delivered to the lake. While most researchers and managers agree that suspended sediments can be mapped with remotely sensed data, the technique with the current spatial resolution of satellite data [100,103] does not allow the detail mapping of water bodies or measurements in or from streams needed for management decisions.

Remote sensing has been used to measure chlorophyll concentrations spatially and temporally. As with suspended sediment measurements, most remote sensing studies of chlorophyll in water are based on empirical relationships between radiance/reflectance in narrow bands or band ratios and chlorophyll. Measurements made in situ [110] show spectra (Fig. 10) with increasing reflectance with increased chlorophyll concentration across most wavelengths but areas of decreased reflectance in the spectral absorption region for chlorophyll (675–680 nm). A variety of algorithms and wavelengths have been used successfully to map chlorophyll concentrations of the oceans, estuaries and fresh waters. While estimating chlorophyll by remote sensing technique is possible, studies have also shown that the broad wavelength spectral data available on current satellites (i.e., Landsat, SPOT) do not permit discrimination of

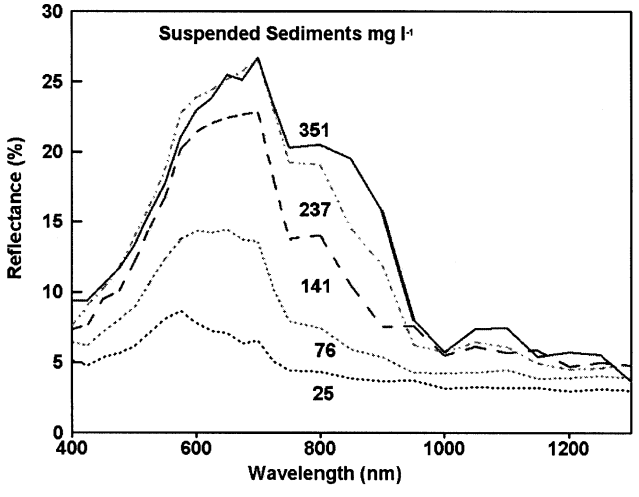

Fig. 9. The relationship between reflectance and wavelength as affected by the concentration of suspended sediments [105].

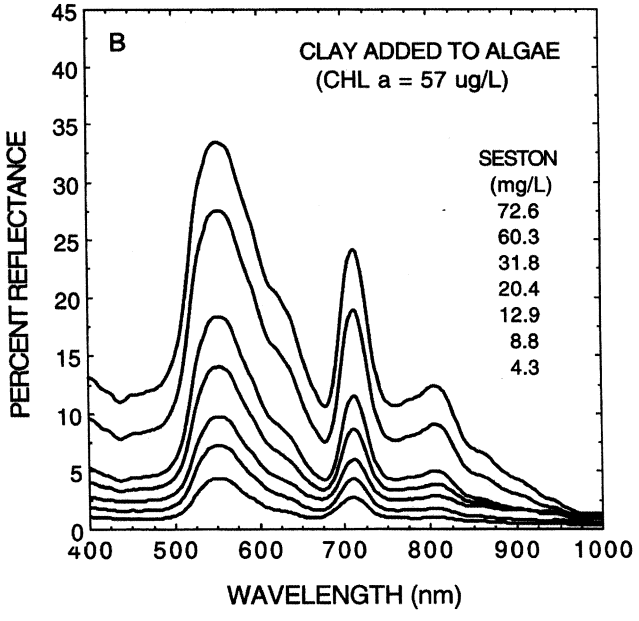

Fig. 10. Relative contributions of chlorophyll and suspended sediment to a reflectance spectra of surface water. Based on in situ laboratory measurements made 1 m above the water surface by Schalles et al. [110].

chlorophyll in waters with high suspended sediments [21,97,104] due to the dominance of the spectral signal from the suspended sediments. Research on the relationship between chlorophyll and the narrow band spectral details at the "red edge" of the visible spectrum [30] has shown a linear relationship between chlorophyll and the difference between the emergent energy in the primarily chlorophyll scattering range (700–705 nm) and the primarily chlorophyll absorption range (675–680 nm). The relationship exists even in the presence of high suspended sediment concentrations that can dominate the remainder of the spectrum as seen in Fig. 10. These findings suggest new approaches for application of airborne and spaceborne sensors to exploit these phenomena to estimate chlorophyll in surface waters under all conditions as hyperspectral sensors are launched and data become available.

While current remote sensing technologies have many actual and potential applications for assessing water resources and for monitoring water quality, limitations in spectral and spatial resolution of many current sensors on satellites currently restrict the wide application of satellite data for monitoring water quality. New satellites (i.e., SEAWIFS, EOS, MOS, IKONOS, etc.) and sensors (hyperspectral, high spatial resolution) already launched or planned to be launched over the next decade will provide the improved spectral and spatial resolutions needed to monitor water quality parameters in surface waters from space platforms. Research needs to focus on understanding the effects of water quality on optical and thermal properties of surface waters so that physically based models can be developed relating water quality parameters to optical measurements made by remote sensing techniques. Hyperspectral data from space platforms will allow us to discriminate between water quality parameters and to develop a better understanding of light/water/substance interactions. Such information should allow us to move away from empirical approaches now being used and develop algorithms that will allow us to use the full resolution electromagnetic spectrum to monitor water quality parameters.

3. Remote sensing of hydrometeorological fluxes

3.1. Evapotranspiration

One of the more common ways in estimating ET is to rearrange Eq. (2) solving for the latent heat flux, LE, as a residual in the energy balance equation for the land surface, namely,

$$LE = R_N - G - H \tag{9}$$

Remote sensing methods for estimating these components are described in [53]. Typically with reliable estimates of solar radiation, differences between remote sensing estimates and observed $R_N - G$ are within 10%.

The largest uncertainty in estimating LE comes from computing H. In resistance form, the relationship between H and the surface-air temperature difference is expressed as

$$H = \rho C_p \frac{T_0 - T_A}{R_A} \tag{10}$$

where T_0 is the aerodynamic surface temperature (T_0 is the temperature satisfying the traditional expressions for the resistances; see [78]), T_A is the near-surface air temperature, is air density, C_p is the specific heat of air, and R_A is the aerodynamic resistance. Since T_0 cannot be measured the surface radiometric temperature is often substituted in Eq. (10) and is frequently rewritten as (e.g., [122]),

$$H = \rho C_p \frac{T_R(\theta) - T_A}{R_A + R_{EX}} \tag{11}$$

where R_{EX} is the so-called "excess resistance", which attempts to account for the non-equivalence of T_0 and $T_R(\theta)$. The radiometric temperature observations, $T_R(\theta)$, at some viewing angle θ, are converted from satellite brightness temperatures and are an estimate of the land surface temperature, T_{SURF}. Thus Eqs. (9)–(11) offer the possibility of mapping surface heat fluxes on a regional scale if R_A and R_{EX} can be estimated appropriately. R_{EX} has been related to the ratio of roughness lengths for momentum, z_{OM}, and heat, z_{OH}, and the friction velocity u_* having the form (e.g., [122]),

$$R_{EX} = k^{-1} \ln\left(\frac{z_{OM}}{z_{OH}}\right) u_*^{-1} \tag{12}$$

where $k \approx 0.4$ is von Karman's constant. This is the classical definition which addresses the fact that momentum and heat transport from the roughness elements differ [10], but is just one of several that have been formulated (e.g., [66]). There have been numerous efforts in recent years to apply Eqs. (11) and (12) and determine the behavior of R_{EX} or z_{OH} for different surfaces, but no universal relation exists [53]. Large spatial and temporal variations in the magnitude of z_{OH} have been found. Nevertheless, solving the LE with the approach summarized in Eqs. (9)–(12) is still widely applied.

It is important to recognize the fact that satellite observations are essentially "instantaneous" or merely "snap shots" of the surface conditions. For many practical applications, LE estimates at longer time scales, namely daily values, are needed. This was the impetuous for an empirical scheme for estimating daily LE, LE_D, [41] using observations of $T_R(\theta)$ and T_A near midday or maximum heating,

$$LE_D = R_{N,D} - B(T_{R,i}(\theta) - T_{A,i})^n \tag{13}$$

where the subscript i and D represent "instantaneous" and daily values, respectively. The coefficients B and n

have been related to physical properties of the land surface and atmosphere namely, z_{OM} and stability, respectively [118]. Both theoretical and experimental studies have evaluated Eq. (13) lending further support for its utility as a simple technique for estimating LE_D [12,13,60]. In fact, studies have applied Eq. (13) to meteorological satellites for longer term regional ET monitoring in the Sahelian regions of Africa and for France [119,120].

However, a major drawback with these approaches summarized above is that there is no distinction made between soil and vegetation canopy components. Hence vegetation water use or stress cannot be assessed. Furthermore, as evidence from many previous studies both the resistances in Eq. (11) and consequently the B parameter in Eq. (13) are not uniquely defined by surface roughness parameters. In addition to experimental evidence (e.g., [124,125]), Kustas et al. [58] using a complex soil-vegetation-atmosphere-transfer (SVAT) model (Cupid [79]) have shown the lack of a unique relationship between $T_R(\theta)$ and the "aerodynamic" surface temperature, T_0.

An alternative approach recently proposed considers the soil and vegetation contribution to the total or composite heat fluxes and soil and vegetation temperatures to the radiometric temperature measurements in a so-called "two-source" modeling (TSM) scheme [80]. This allows for Eq. (10) to be recast into the following expression:

$$H = \rho C_p \frac{T_R(\theta) - T_A}{R_R} \tag{14}$$

where R_R is the radiometric-convective resistance given by [80],

$$R_R = \frac{T_R(\theta) - T_A}{\dfrac{T_C - T_A}{R_A} + \dfrac{T_S - T_A}{R_A + R_S}}. \tag{15}$$

T_C is the canopy temperature, T_S is the soil temperature, and R_S is the soil resistance to heat transfer. An estimate of leaf area index or fractional vegetation cover, f_C, is used to estimate T_C and T_S from $T_R(\theta)$,

$$T_R(\theta) \approx \left(f_C(\theta) T_C^4 + (1 - f_C(\theta)) T_S^4\right)^{1/4} \tag{16}$$

where $f_C(\theta)$ is the fractional vegetative cover at radiometer viewing angle θ, and R_S is computed from a relatively simple formulation predicting wind speed near the soil surface [80]. With some additional formulations for estimating canopy transpiration, and the dual requirement of energy and radiative balance of the soil and vegetation components, closure in the set of equations is achieved. Through model validation studies, revisions to the original two-source formulations have been made [56–59] which improved the reliability of flux estimation under a wider range of environmental conditions. The modifications include: (i) replacing the commonly used Beer's Law expression for estimating the divergence of the net radiation through the canopy layer with a more physically based algorithm; (ii) adding a simple method to address the effects of clumped vegetation on radiation divergence and wind speed inside the canopy layer, and radiative temperature partitioning between soil and vegetation components; (iii) a scheme for adjusting the magnitude of the Priestley–Taylor [89] coefficient, α_{pt}, used in estimating canopy transpiration for advective and stressed canopy conditions; and (iv) developing a new soil aerodynamic resistance formulation whose magnitude is a function of both convective (temperature) and mechanical (wind) turbulent transport.

Earlier studies recognized the need to consider fractional vegetation cover on ET using information provided in the vegetation index-radiometric temperature, VI-$T_R(\theta)$, space [88]. He used an energy balance model for computing spatially distributed fluxes from the variability within the normalized difference vegetation index NDVI-$T_R(\theta)$ space from a single satellite scene. NDVI was used to estimate the fraction of a pixel covered by vegetation and showed how one could derive bare soil and vegetation temperatures and, with enough spatial variation in surface moisture, estimate daily ET for the limits of full cover vegetation, dry and wet bare soils.

Following Price [88] and Carlson et al. [14,15] combined an atmospheric boundary layer (ABL) model with a SVAT for mapping surface soil moisture, vegetation cover and surface fluxes. Model simulations are run for two conditions: 100% vegetative cover with the maximum NDVI being known a priori, and with bare soil conditions knowing the minimum NDVI. Using ancillary data (including a morning sounding, vegetation and soil type information) root-zone and surface soil moisture are varied, respectively, until the modeled and measured $T_R(\theta)$ are closely matched for both cases so that fractional vegetated cover and surface soil moisture are derived. Further refinements to this technique have been developed by Gillies and Carlson [29] for potential incorporation into climate models. Comparisons between modeled-derived fluxes and observations have been made recently by Gillies et al. [28] indicating approximately 90% of the variance in the fluxes were captured by the model.

In a related approach, Moran et al. [70,74] defined theoretical boundaries in VI-$(T_R(\theta) - T_A)$ space using the Penman–Monteith equation in order to extend the application of the crop water stress index to partial vegetation cover (see below). The boundaries define a trapezoid, which has at the upper two corners unstressed and stressed 100% vegetated cover and at the lower two corners, wet and dry bare soil conditions. In order to calculate the vertices of the trapezoid, measurements of R_N, vapor pressure, T_A, and wind speed are required as well as vegetation specific parameters; these include

maximum and minimum VI for the full-cover and bare soil case, maximum leaf area index, and maximum and minimum stomatal resistance. Moran et al. [70] analyze and discuss several of the assumptions underlying the model, especially those concerning the linearity between variations in canopy-air temperature and soil-air temperatures and transpiration and evaporation. Information about *ET* rates are derived from the location of the VI-($T_R(\theta) - T_A$) measurements within the date and time-specific trapezoid. This approach permits the technique to be used for both heterogeneous and uniform areas and thus does not require having a range of NDVI and surface temperature in the scene of interest as required by Carlson et al. [15] and Price [88]. Moran et al. [70] have compared the method for estimating relative rates of *ET* with observations over agricultural fields and showed it could be used for irrigation scheduling purposes. More recently, Moran et al. [71] have shown the technique has potential for computing *ET* over natural grassland ecosystems.

All these modeling schemes however, are susceptible to errors in the radiometric temperature observations and most require screen level meteorological inputs (primarily wind speed, u, and air temperature, T_A, observations) which at regional scales suffer from errors of representativeness. Approaches using remotely sensed data for estimating the variation of these quantities are being developed and tested [6,7,26]. How reliable the algorithms are for different climatic regimes needs to be evaluated.

A modeling framework has recently been developed to address these limitations [4,67] through an energy closure scheme, Atmospheric-Land-EXchange-Inverse (ALEXI) which employs the TSM approach [80] to also address the non-uniqueness of the radiometric–aerodynamic temperature relationship. ALEXI uses the growth of the ABL, a quantity sensitive to heat flux input to the lower atmosphere, and coupling this growth to the temporal changes in surface radiometric temperature from the geosynchronous operational environmental satellite (GOES). Using temporal changes of brightness temperatures, errors in the conversion to radiometric surface temperatures are significantly mitigated. The use of an energy balance method involving the temporal change of the height of the ABL moderates errors that arise in schemes that utilize the surface-air temperature gradient for estimating the heat fluxes since the ALEXI model derives local air temperature at an interface height of ≈50 m.

Another much simpler scheme, which also uses the TSM framework, employs the time rate of change in radiometric temperature and air temperature observations from a nearby weather station in a simple formulation for computing regional heat fluxes, called the dual-temperature-difference (DTD) approach [81]. Although this technique requires air temperature observations, by using a time difference in air temperature, errors caused by using local shelter level observations for representing a region are still reduced. Moreover, the scheme is simple, thus it is computationally efficient and does not require atmospheric sounding data for initialization. Preliminary comparisons of regional scale *ET* output over the central US between DTD and the more computational intensive and complex ALEXI scheme show good agreement in the patterns [59].

An example of application of the TSM approach for estimating daily ET is illustrated in Figs. 11 and 12 for the September 4, 2000 ASTER data. Images of $T_R(\theta)$ and NDVI computed from the ASTER red and near-infrared reflectance data and the multi-spectral TIR data are given in Fig. 11 [25]. The NDVI image shows bare soil with values ∼0.0 (light gray) and senescent grazing lands with values ∼0.2 (dark gray). Surface temperature imagery distinguishes bare soils, at

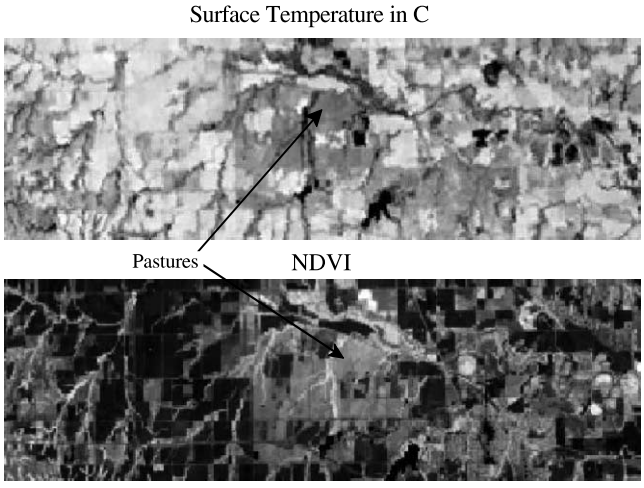

Fig. 11. Surface temperatures and NDVI values for the portion of Fig. 1 outlined by the white box. The area is ≈30 × 8 km. The temperatures range from 36 to 57 °C and the ndvi values range from −0.1 to 0.5.

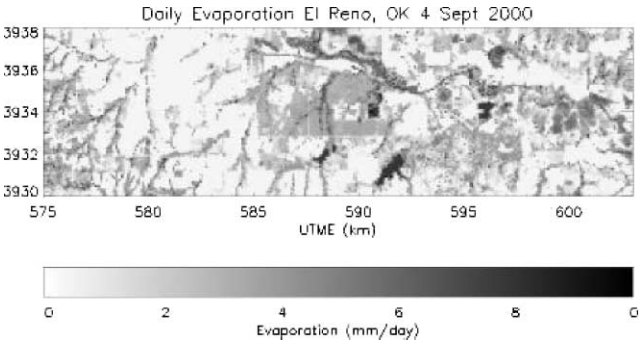

Fig. 12. Estimated daily evapotranspiration over the El Reno, Oklahoma study area using ASTER observation at about 11:30 am. A drought occurred during the summer of 2000, and by September many of the fields were either plowed or contained senescent vegetation. In this image, 0–1 corresponds to dry soils, 4 to grass lands, and 68 to lakes, ponds and riparian zones.

55–60 °C (light gray), from grazing lands, at ~45 °C (medium gray). These remote sensing inputs, in combination with TSM, resulted in 90 m scale estimates of H and LE. Comparison with ground-based energy balance observations using the Bowen ratio technique show underestimated H and Rn, but close agreement for LE. Assuming constant daytime evaporative fraction, instantaneous values can be integrated to yield daily evaporative flux estimates given in Fig. 12. The latter range from about 5 mm/day for the grazing lands and 8 mm/day for the water bodies. Many of the low ET rates are from fields that are either bare soil or contain wheat stubble from the summer winter wheat harvests, which generally have the highest $T_R(\theta)$ and $0 \leqslant \mathrm{NDVI} \leqslant 0.1$. Higher ET rates come from grassland sites ($\mathrm{NDVI} \geqslant 0.2$) with the highest rates over irrigated crop fields and riparian areas along streams where $\mathrm{NDVI} \geqslant 0.4$ and water bodies where $\mathrm{NDVI} \leqslant 0$ (Fig. 11).

4. Concluding remarks

Algorithm and model development with existing and new remote sensing technologies for assessing hydrometeorological state variables and fluxes is considered critical since this is the only technology available that can ultimately provide the capability to monitor crop development and yield via stress indicators and plant water use over a range of spatial scales, from field, farm, and watershed, up to regional scales. To attain this goal, new research directions to address science questions impeding hydrometeorological research.

One area is in developing a framework for combining multi-frequency remote sensing information, from the visible to microwave wavelengths for more reliable estimation of vegetation and soil properties and states. There is empirical and theoretical evidence that SAR backscatter in combination with optical data (i.e., visible, through TIR wavelengths) may provide useful information about crop water stress [72,73]. At high frequencies (~13 GHz), field experiments have shown that the radar signal was particularly sensitive to such plant parameters as leaf area index, plant biomass, and percentage of vegetation cover. At low frequencies (~5 GHz), many studies have shown that the radar signal is very sensitive to soil moisture, though this sensitivity decreased with increasing vegetation cover.

In a related approach, remotely sensed near-surface moisture from a passive microwave sensor has been used in combination with optical data for estimating the soil and vegetation energy balance. The model has been applied over a semiarid area in southern Arizona [55], and in the Southern Great Plains in Oklahoma [54]. Comparison of model computed ET with ground- and aircraft-based observations showed good results, with discrepancies between modeled and observed ET averaging ~15%. It is also shown that it may be possible to simulate the daytime fluxes with only a single microwave observation.

Another important area related to scaling up from field to regional scales, is the effects of landscape heterogeneity on atmospheric dynamics and mean air properties and resulting feedbacks on the land surface fluxes. This can be captured in a modeling framework using large eddy simulation (LES). LES models simulate the space and time dynamics of ABL turbulence and the interactions with the land surface using a numerical solution of the Navier–Stokes equations (e.g., [2]). However, most studies to date addressing land surface heterogeneity using LES have described surface boundary conditions as predefined fluxes with artificial variability or with spatial variability defined to match the surface flux fields estimated from experimental data at a particular site. The questions of how the surface heterogeneity affects ABL heterogeneity, and how the surface and air properties in turn affect the flux fields that develop over a region with heterogeneous surface properties are left unanswered in most LES studies.

The LES-remote sensing model recently developed by Albertson et al. [3] couples remotely sensed surface temperature and soil moisture fields (2D) to the dynamic (4D) ABL variables via the TSM scheme described earlier; hence, separate and explicit contributions from soil and vegetation (i.e., two sources) to mass and energy exchanges are included. This is a merger of active lines of research: the use of remotely sensed land surface properties to study water and energy fluxes, and the use of LES to study the impacts of surface variability on ABL processes. This LES-remote sensing model can run over a ~10 km^2 domain at relatively high spatial resolution (~100 m) with remotely sensed vegetation cover, surface soil moisture and temperature defining surface heterogeneities governing atmospheric exchanges/interactions with the land surface. Typically, land–atmosphere models are either driven by a network of surface meteorological observations, or use energy conservation principles applied to ABL dynamics to deduce air temperature [4]. However, neither approach considers the resulting impact/feedback of surface heterogeneity on atmospheric turbulence and the resulting spatial features of the mean air properties, particularly at the patch or local scale. The predictions from the LES-remote sensing modeling scheme will provide a benchmark for assessing the impact of a range of surface heterogeneity features on land–atmosphere predictions neglecting such coupling.

References

[1] Ahmed NU. Estimating soil moisture from 6.6 GHz dual polarization, and/or satellite derived vegetation index. Int J Remote Sens 1995;16:687–708.

[2] Albertson JD, Parlange MB. Natural integration of scalar fluxes from complex terrain. Adv Water Resour 1999;23:239–52.
[3] Albertson JD, Kustas WP, Scanlon TM. Large eddy simulation over heterogeneous terrain with remotely sensed land surface conditions. Water Resour Res 2001;37(7):1939–53.
[4] Anderson MC, Norman JM, Diak GR, Kustas WP. A two-source time Integrated model for estimating surface fluxes for thermal infrared satellite observations. Remote Sens Environ 1997;60:195–216.
[5] Armstrong RL, Chang A, Rango A, Josberger E. Snow depths and grain-size relationships with relevance for passive microwave studies. Ann Glaciol 1993;17:171–6.
[6] Bastiaanssen WGM, Menenti M, Feddes RA, Holtslag AAM. A remote sensing surface energy balance algorithm for land (SEBAL) 1. Formulation. J Hydrol 1998;212–213:198–212.
[7] Bastiaanssen WGM, Pelgrum H, Wang Y, Ma Y, Moreno JF, Roerink GJ, et al. A remote Sensing surface energy balance algorithm for land (SEBAL) 2. Validation. J Hydrol 1998;212–213:213–29.
[8] Becker F, Li Z-L. Towards a local split window over land surfaces. Int J Remote Sens 1990;11:369–93.
[9] Berk A, Bernstein LS, Anderson GP, Acharya PK, Robertson DC, Chetwynd JH, et al. MODTRAN cloud and multiple scattering upgrade with application to AVIRIS. Remote Sens Environ 1998;65:367–75.
[10] Brutsaert W. Evaporation into the atmosphere, theory, history and applications. Norwell, Massachusetts: D. Reidel, Norwell; 1982.
[11] Burke EJ, Gurney RJ, Simmonds LP, O'Neill PE. Using a modeling approach to predict soil hydraulic properties from passive microwave measurements. IEEE Trans Geosci Remote Sens 1998;36:454–62.
[12] Carlson TN, Buffum MJ. On estimating total daily evapotranspiration from remote surface measurements. Remote Sens Environ 1989;29:197–207.
[13] Carlson TN, Capehart WJ, Gillies RR. A new look at the simplified method for remote sensing of daily evapotranspiration. Remote Sens Environ 1995;54:161–7.
[14] Carlson TN, Gillies RR, Perry EM. A method to make use of thermal infrared temperature and NDVI measurements to infer soil water content and fractional vegetation cover. Remote Sens Rev 1994;52:45–59.
[15] Carlson TN, Perry EM, Schmugge TJ. Remote estimation of soil moisture availability and fractional vegetation cover for agricultural fields. Agric Forest Meteorol 1990;52:45–69.
[16] Chang ATC, Foster JL, Hall DK. Nimbus-7 SMMR derived global snow cover parameters. Ann Glaciol 1987;9:39–44.
[17] Choudhury BJ, Golus RE. Estimating soil wetness using satellite data. Int J Remote Sens 1988;9:1251–7.
[18] Choudhury BJ, Schmugge TJ, Chang ATC, Newton RW. Effect of surface roughness on the microwave emission of soils. J Geophys Res 1979;84:5699–705.
[19] Curran PJ, Novo EMM. The relationship between suspended sediment concentration and remotely sensed spectral radiance: a review. J Coast Res 1988;4:351–68.
[20] Coll C, Caselles V. A split-window algorithm for land surface temperature from AVHRR data: validation and algorithm comparison. J Geophys Res 1997;102(D14):16697–712.
[21] Dekker AG, Peters SWM. The use of the Thematic Mapper for the analysis of eutrophic lakes: a case study in the Netherlands. Int J Remote Sens 1993;14(5):799–821.
[22] Dobson MC, Ulaby FT, Hallikainen MT, El-Rayes MA. Microwave dielectric behavior of wet soil, II, Dielectric mixing models. IEEE Trans Geosci Remote Sens 1985;GE-23:35–46.
[23] Foster JL, Rango A. Snow cover conditions in the northern hemisphere during the winter of 1981. J Climate 1982;20:171–83.
[24] French AN, Schmugge TJ, Kustas WP. Discrimination of senescent vegetation using thermal emissivity contrast. Remote Sens Environ 2000b;74:249–54.
[25] French AN, Schmugge TJ, Kustas WP. Estimating evapotranspiration over El Reno Oklahoma with ASTER imagery. Agronomie: Agric Environ 2002;22:105–6.
[26] Gao W, Coultier RL, Lesht BM, Qui J, Wesely ML. Estimating clear-sky regional surface fluxes in the southern Great Plains atmospheric radiation measurement site with ground measurements and satellite observations. J Appl Meteorol 1998;37:5–22.
[27] Gillespie A, Rokugawa S, Matsunaga T, Cothern JS, Hook S, Kahle AB. A temperature and emissivity separation algorithm for advanced spaceborne thermal emission and reflection radiometer (ASTER) images. IEEE Trans Geosci Remote Sens 1998;36:1113–26.
[28] Gillies RR, Carlson TN, Cui J, Kustas WP, Humes KS. Verification of the 'triangle' method for obtaining surface soil water content and energy fluxes from remote measurements of Normalized Difference Vegetation Index (NDVI) and surface radiant temperature. Int J Remote Sens 1997;18:3145–66.
[29] Gillies RR, Carlson TN. Thermal remote sensing of surface soil water content with partial vegetation cover for incorporation into climate models. J Appl Meteorol 1995;34:745–56.
[30] Gitelson A, Mayo M, Yacobi YZ, Paroarov A, Berman T. The use of high spectral resolution radiometer data for detection of low chlorophyll concentrations in Lake Kinneret. J Plankton Res 1994;16:993–1002.
[31] Gomez-Landesa E. Evaluacion de Recursos de Agua en Forma de Nieve mediante Teledeteccion usando satelites de la sine NOAA (Evaluation of water resources in the form of snow by remote sensing using NOAA satellites). PhD thesis, Universidad Politenica de Madrid, Madrid, Spain, 1997.
[32] Gomez-Landesa E, Rango A. Snow cover remote sensing and snowmelt runoff forecasts in the Spanish Pyrenees using the SRM model. In: Proceedings of the Fourth International Workshop on Applications of Remote Sensing in Hydrology, NHRI Symposium Report, Santa Fe, NM, 1998. 12pp.
[33] Gomez-Landesa E, Rango A. Assessment of MODIS channels 1and 2 snow cover mapping capability. EOS Trans Am Geophy Union 2000;81(48):F548.
[34] Goodell BC. Snowpack management for optimum water benefits. ASCE Water Resources Engineering Conference, Denver, Colorado: Conference Preprint 379, 1966.
[35] Goodison BE. Determination of areal snow water equivalent on the Canadian prairies using passive microwave satellite data. Proc IGARSS 89, IEEE 1989:1243–6.
[36] Goodison BE, Walker AE. Canadian development and use of snow cover information from passive microwave satellite data. In: Choudhury BJ, Kerr YH, Njoku EG, Pampaloni P, editors. Passive microwave remote sensing of land–atmosphere interactions. Utrecht, The Netherlands: VSP; 1995. p. 245–62.
[37] Goodison BE, Rubinstein I, Thirkettle FW, Langham EJ. Determination of snow water equivalent on the Canadian prairies using microwave radiometry. In: Modelling Snowmelt Induced Processes, IAHS Publication No. 155, 1986. p. 163–73.
[38] Hall DK. Influence of depth hoar on microwave emission from snow in northern Alaska. Cold Regions Sci Technol 1987;13:225–31.
[39] Hallikainen M, Jolma P. Development of algorithms to retrieve the water equivalent of snow cover from satellite microwave radiometer data. In: Proc 1986 International Geoscience and Remote Sensing Symposium (IGARSS 86), Zurich, Switzerland. 1986. p. 611–6.
[40] Harding DJ, Bufton JL, Frawley JJ. Satellite lidar altimetry of terrestrial topography: Vertical accuracy as a function of surface slope, roughness, and cloud cover. IEEE Trans Geosci Remote Sens 1994;32:329–39.

[41] Jackson RD, Reginato RJ, Idso SB. Wheat canopy temperature: A practical tool for evaluating water requirements. Water Resour Res 1977;13:651–6.
[42] Jackson TJ, Schmugge TJ. Passive microwave remote sensing system for soil moisture: Some supporting research. IEEE Trans Geosci Remote Sens 1989;27:225–35.
[43] Jackson TJ, Schmugge TJ. Vegetation effects on the microwave emission from soils. Remote Sens Environ 1991;36:203–12.
[44] Jackson TJ, Schmugge TJ, Wang JR. Passive microwave remote sensing of soil moisture under vegetation canopies. Water Resour Res 1982;18:1137–42.
[45] Jackson TJ, Le Vine DM, Swift CT, Schmugge TJ, Schiebe FR. Large area mapping of soil moisture using the ESTAR passive microwave radiometer in Washita'92. Remote Sens Environ 1995;53:27–37.
[46] Jackson TJ, McNairn H, Weltz MA, Brisco B, Brown R. First order surface roughness correction of active microwave observations for estimating soil moisture. IEEE Trans Geosci Remote Sens 1997;35:1065–9.
[47] Jackson TJ, Le Vine DM, Hsu AY, Oldak A, Starks PJ, Swift CT, et al. Soil moisture mapping at regional scales using microwave radiometry: the Southern Great Plains hydrology experiment. IEEE Trans Geosci Remote Sens 1999;37:2136–51.
[48] Kerr YH, Lagouarde JP, Imberon J. Accurate land surface temperature retrieval from AVHRR data with use of an improved split window algorithm. Remote Sens Environ 1992;41:197–209.
[49] Kerr Y, Waldteufel P, Wigneron J-P, Martinuzzi J-M, Font J, Berger M. Soil Moisture retrieval from space: The Soil Moisture and Ocean Salinity (SMOS) Mission. IEEE Trans Geosci Remote Sens 2001;GE-39:1729–35.
[50] Krajewski WF, Smith J, Foufoula E. Rainfall measurement and modeling. Adv Water Res (this volume).
[51] Kunzi KF, Patil S, Rott H. Snow cover parameters retrieved from Nimbus-7 Scanning Mutlichannel Microwave Radiometers (SMMR) data. IEEE Trans Geosci Remote Sens 1982;GE-20(4):452–67.
[52] Kustas WP, Blanford JH, Stannard DI, Daughtry CST, Nichols WD, Weltz MA. Local energy flux estimates for unstable conditions using variance data in semiarid rangelands. Water Resour Res 1994;30(5):13511361.
[53] Kustas WP, Norman JM. Use of remote sensing for evapotranspiration monitoring over land surfaces. Hydrol Sci J des Sci Hydrol 1996;41:495–516.
[54] Kustas WP, Zhan X, Jackson TJ. Mapping surface energy flux partitioning at large scales with optical and microwave remote sensing data from Washita'92. Water Resour Res 1999;35:265–77.
[55] Kustas WP, Zhan X, Schmugge TJ. Combining optical and microwave remote sensing for mapping energy fluxes in a semiarid watershed. Remote Sens Environ 1998;64:116–31.
[56] Kustas WP, Norman JM. Evaluation of soil and vegetation heat flux predictions using a simple two-source model with radiometric temperatures for partial canopy cover. Agric Forest Meteorol 1999;94:13–29.
[57] Kustas WP, Norman JM. Evaluating the effects of sub-pixel heterogeneity on pixel average fluxes. Remote Sen Environ 2000;74:327–42.
[58] Kustas WP, Norman JM, Schmugge TJ, Anderson MC. Mapping surface energy fluxes with radiometric temperature. In: Quattrochi DA, Luvall JC, editors. Thermal remote sensing in land surface processes. Taylor & Francis; in press.
[59] Kustas WP, Diak GR, Norman JM. Time difference methods for monitoring regional scale heat fluxes with remote sensing. In: Observations and modeling of the land surface hydrological processes. American geophysical union water science and applications series, vol. 3. 2001. p. 1529.
[60] Lagouarde J-P. Use of NOAA AVHRR data combined with an agrometeorological model for evaporation mapping. Int J Remote Sens 1991;12:1853–64.
[61] Lal R. Soil erosion. Ankeny, Iowa: Soil and Water Conservation Society; 1994.
[62] Le Vine DM, Griffis A, Swift CT, Jackson TJ. ESTAR: a synthetic microwave radiometer for remote sensing applications. Proc IEEE 1994;82:1787–801.
[63] Link LE. Capability of airborne lidar profilometer system to measure terrain roughness. In: Proceedings 6th Symposium Remote Sensing Environment, Ann Arbor, Michigan. 1969. p. 189–96.
[64] Martinec J, Rango A, Roberts R. Snowmelt Runoff Model (SRM) user's manual. Geographica Bernensia P35, Department of Geography, University of Berne, 1998. 84pp.
[65] McCuen RH, Snyder WM. Hydrologic modeling: statistical methods and applications. Englewood, NJ: Prentice-Hall; 1986. 568pp.
[66] McNaughton KG, Van den Hurk BJJM. A 'Lagrangian' revision of the resistors in the two-layer model for calculating the energy budget of a plant canopy. Boundary-Layer Meteorol 1995;74: 262–88.
[67] Mecikalski JR, Diak GR, Anderson MC, Norman JM. Estimating fluxes on continental scales using remotely-sensed data in an atmospheric-land exchange model. J Appl Meteorol 1999;38: 1352–69.
[68] Menenti M, Ritchie JC. Estimation of effective aerodynamic roughness of Walnut Gulch watershed with lidar altimeter measurements. Water Resour Res 1994;30:1329–37.
[70] Moran MS, Clarke TR, Inoue Y, Vidal A. Estimating crop water deficit using the relation between surface-air temperature and spectral vegetation index. Remote Sens Environ 1994;49:246–63.
[71] Moran MS, Rahman AF, Washburne JC, Goodrich DC, Weltz MA, Kustas WP. Combining the Penman–Monteith equation with measurements of surface temperature and reflectance to estimate evaporation rates of semiarid grassland. Agric Forest Meteorol 1996;80:87–109.
[72] Moran MS, Vidal A, Troufleau D, Qi J, Clarke TR, Pinter Jr PJ, et al. Combining multifrequency microwave and optical data for crop management. Remote Sens Environ 1997;61:96–109.
[73] Moran MS, Vidal A, Troufleau D, Inoue Y, Mitchell TA. Ku- and C-band SAR for discriminating agricultural crop and soil conditions. IEEE Geosci Remote Sens 1998;36:265–72.
[74] Moran MS. Thermal responses as indicators of biophysical system health and integrity. In: Luvall J, Quattrochi D, editors. Thermal remote sensing in land surface processes. Taylor & Francis; in press.
[75] Newton RW, Black QR, Makanvand S, Blanchard AJ, Jean BR. Soil moisture information and thermal microwave emission. IEEE Trans Geosci Remote Sens 1982;GE-20:275–81.
[76] Njoku EG, Kong J. Theory for passive microwave remote sensing of near-surface soil moisture. J Geophys Res 1977;82: 3108–18.
[77] Njoku EG, Li L. Retrieval of land surface parameters using passive microwave measurements at 6 to 18 GHz. IEEE Trans Geosci Remote Sens 1999;37:79–93.
[78] Norman JM, Becker F. Terminology in thermal infrared remote sensing of natural surfaces. Remote Sens Rev 1995;12:159–73.
[79] Norman JM, Campbell GS. Application of a plant-environment model to problems in irrigation. In: Hillel DI, editor. Advances in irrigation, vol. II. New York: Academic Press; 1983. p. 155–88.
[80] Norman JM, Kustas WP, Humes KS. A two-source approach for estimating soil and vegetation energy fluxes from observations of directional radiometric surface temperature. Agric Forest Meteorol 1995;77:263–93.
[81] Norman JM, Daniel LC, Diak GR, Twine TE, Kustas WP, French AN, et al. Satellite estimates of evapotranspiration

on the 100-m pixel scale. IEEE IGARRS 2000 Proc 2000;IV: 1483–5.
[82] Owe M, van de Griend AA, Chang ATC. Surface soil moisture and satellite microwave observations in semiarid southern Africa. Water Resour Res 1992;28:829–39.
[83] Pachepsky YA, Ritchie JC. Seasonal changes in fractal landscape surface roughness estimated from airborne laser altimetry data. Int J Remote Sens 1998;19(13):2509–16.
[84] Pachepsky YA, Ritchie JC, Gimenez D. Fractal modeling of airborne laser altimetry data. Remote Sens Environ 1997;61:150–61.
[85] Prata AJ. Land surface temperature derived from the advanced very high resolution radiometer and the along-track scanning radiometer 2. Experimental results and validation of AVHRR algorithms. J Geophys Res 1994;99(D6):13025–58.
[86] Price JC. Estimating surface temperatures from satellite thermal infrared data. A simple formulation for the atmospheric effect. Remote Sens Environ 1983;13:353–61.
[87] Price JC. Land surface temperature measurements from the split window bands of the NOAA 7 advanced very high resolutions radiometer. J Geophys Res 1984;89:7231–7.
[88] Price JC. Using spatial context in satellite data to infer regional scale evapotranspiration. IEEE Trans Geosci Remote Sens 1990;GE-28:940–8.
[89] Priestley CHB, Taylor RJ. On the assessment of surface heat flux and evaporation using large-scale parameters. Monthly Weath Rev 1972;100:81–92.
[90] Rango A, Chang ATC, Foster JL. The utilization of spaceborne microwave radiometers for monitoring snowpack properties. Nordic Hydrol 1979;10:25–40.
[91] Rango A. The snowmelt-runoff model. Proc. ARS Natural Res. Modeling symp. Pingree Park, CO, USDA-ARS-30, 1985. p. 321–5.
[92] Rango A, Chopping M, Ritchie J, Havstad K, Kustas W, Schmugge T. Morphological characteristics of shrub coppice dunes in desert grasslands of southern New Mexico derived from scanning lidar. Remote Sens Environ 2000;74:26–44.
[93] Rango A, Martinec J, Chang ATC, Foster JL, van Katwijk V. Average areal water equivalent of snow in a mountain basin using microwave and visible satellite data. IEEE Trans Geosci Remote Sens 1989;GE-27(6):740–5.
[94] Ritchie JC. Remote sensing applications to hydrology: airborne lidar altimeters. Hydrol Sci J 1996;41(4):625–36.
[95] Ritchie JC, Evans DL, Jacobs DM, Everitt JH, Weltz MA. Measuring canopy structure with an airborne lidar altimeter. Trans Am Soc Agric Eng 1993;36:1235–8.
[96] Ritchie JC, Everitt JH, Escobar DE, Jackson TJ, Davis MR. Airborne lidar measurements of rangeland canopy cover. J Range Manage 1992;45:189–93.
[97] Ritchie JC, Grissinger EH, Murphey JB, Garbrecht JD. Measuring channel and gully cross-sections with an airborne lidar altimeter. Hydrol Process J 1994;7:237–44.
[98] Ritchie JC, Jackson TJ. Airborne laser measurement of the topography of concentrated flow gullies. Trans Am Soc Agric Eng 1989;32:645–8.
[99] Ritchie JC, Seyfried MS, Chopping MJ, Pachepsky Y. Airborne laser technology for measuring rangeland conditions. J Range Manage 2001;54(2):A8–A21.
[100] Ritchie JC. Soil erosion. In: Schultz GA, Engman ET, editors. Remote sensing in hydrology and water management. Berlin, Germany: Springer-Verlag; 2000. p. 271–86, 349–50.
[101] Ritchie JC, Cooper CM. An algorithm for using Landsat MSS for estimating surface suspended sediments. Water Resour Bull 1991;27:373–9.
[102] Ritchie JC, Cooper CM. Comparison on measured suspended sediment concentrations with suspended sediment concentrations estimated from Landsat MSS data. Int J Remote Sens 1988;9:379–87.
[103] Ritchie JC, Schiebe FR. Water quality. In: Schultz GA, Engman ET, editors. Remote sensing in hydrology and water management. Berlin, Germany: Springer-Verlag; 2000. p. 287–303, 351–2.
[104] Ritchie JC, Schiebe FR, Cooper CM, Harrington Jr JA. Chlorophyll measurements in the presence of suspended sediment using broad band spectral sensors aboard satellites. J Freshwater Ecol 1994;9(2):197–206.
[105] Ritchie JC, Schiebe FR, McHenry JR. Remote sensing of suspended sediment in surface water. Photogram Eng Remote Sens 1976;42:1539–45.
[106] Robin G. Mapping the Antarctic ice sheet by satellite altimetry. Can J Earth Sci 1966;3:893–901.
[107] Robinson AR. Sediment: Our greatest pollutant. J Soil Water Conservat 1971;53(8):406–8.
[108] Rodriguez-Iturbe I, Vogel GK, Rigon R, Entekhabi D, Castelli F, Rinaldo A. On the spatial organization of soil moisture fields. Geophys Res Lett 1995;22:2757–60.
[109] Rott H. Capabilities of micorwave sensors for monitoring areal extent and physical properties of the snowpack. In: Sorooshian S, Gupta HV, Rodda SC, editors. Land surface processes in hydrology. NATO ASI series on global environmental change, vol. 46. Berlin: Springer-Verlag; 1997. p. 135–67.
[110] Schalles JF, Schiebe FR, Starks PJ, Troeger WW. Estimation of algal and suspended sediment loads (singly and combined) using hyperspectral sensors and integrated mesocosm experiments. In: Fourth International Conference on Remote Sensing for Marine and Coastal Environments, Orlando, FL. 1997. p. 111–20.
[111] Schmugge T, Gloersen P, Wilheit TT, Geiger F. Remote sensing of soil moisture with microwave radiometers. J Geophys Res 1974;79(2):317–23.
[112] Schmugge TJ. Effect of texture on microwave emission from soils. IEEE Trans Geosci Remote Sens 1980;GE-18:353–61.
[113] Schmugge T, Jackson TJ, Kustas WP, Wang JR. Passive microwave remote sensing of soil moisture: results from HAPEX, FIFE and MONSOON90. ISPRS J Photogram Remote Sensing 1992;47:127–43.
[114] Schmugge TJ, Jackson TJ. Mapping surface soil moisture with microwave radiometers. Meteorol Atmos Phys 1994;54:213–23.
[115] Schmugge T, Hook SJ, Coll C. Recovering surface temperature and emissivity from thermal infrared multispectral data. Remote Sens Environ 1998;65:121–31.
[117] Schmugge T, French A, Ritchie JC, Rango A, Pelgrum H. Temperature and emissivity separation from multispectral thermal infrared observations. Remote Sens Environ 2002;79(2–3):189–98.
[118] Seguin B, Itier B. Using midday surface temperature to estimate daily evaporation from satellite thermal IR data. Int J Remote Sens 1983;4:371–83.
[119] Seguin B, Assad E, Freaud JP, Imbernon J, Kerr YH, Lagouarde J-P. Use of meteorological satellites for rainfall and evaporation monitoring. Int J Remote Sens 1989;10:847–54.
[120] Seguin B, Lagouarde J-P, Saranc M. The assessment of regional crop water conditions from meteorological satellite thermal infrared data. Remote Sens Environ 1991;35:141–8.
[121] Stepphun H. Snow and agriculture. In: Gray DM, Male DN, editors. Handbook of snow: principles, processes, management and use. Toronto: Pergamon Press; 1981. p. 60–125.
[122] Stewart JB, Kustas WP, Humes KS, Nichols WD, Moran MS, de Bruin HAR. Sensible heat flux-radiometric surface temperature relationship for eight semiarid areas. J Appl Meteorol 1994;33:1110–7.
[123] Storr D. Precipitation variations in a small forested watershed. In: Proc 35th Annual Western Snow Conference. 1967. p. 11–6.

[124] Verhoef A, De Bruin HAR, Van den Hurk BJJM. Some practical notes on the parameter kB-1 for sparse vegetation. J Appl Meteorol 1997;36:560–72.
[125] Vining RC, Blad BL. Estimation of sensible heat flux from remotely sensed canopy temperatures. J Geophys Res 1992; 97(D17):18951–4.
[126] Walker AE, Goodison BE. Discrimination of a wet snow cover using passive microwave satellite data. Ann Glaciol 1993;17:307–11.
[127] Walker A, Goodison B, Davey M, Olson D. Atlas of Southern Canadian Prairies Winter Snow Cover from Satellite Passive Microwave Data: November 1978 to March 1986. Atmospheric Environment Service, Environment Canada, 1995.
[128] Wan Z-M, Dozier J. Land surface temperature measurement from space: Physical principles and inverse modeling. IEEE Trans Geosci Remote Sens 1989;27:268–78.
[129] Wan Z, Dozier JA. Generalized split-window algorithm for retrieving land-surface temperature for space. IEEE Trans Geosci Remote Sens 1996;34:892–905.
[130] Wang JR, Schmugge TJ. An empirical model for the complex dielectric permittivity of soils as a function of water content. IEEE Trans Geosci Remote Sens 1979;GE-18:288–95.
[131] Wang JR. Effect of vegetation on soil moisture sensing observed from orbiting microwave radiometers. Remote Sens Environ 1985;17:141–51.
[132] Wang JR. Microwave emission from smooth bare fields and soil moisture sampling depth. IEEE Trans Geosci Remote Sens 1987;GE-25(5):616–22.
[133] Weltz MA, Ritchie JC, Fox HD. Comparison of lidar and field measurements of vegetation heights and canopy cover. Water Resour Res 1994;30:1311–9.
[134] Wigneron J-P, Chanzy A, Calvet J-C, Bruguier N. A simple algorithm to retrieve soil moisture and vegetation biomass using passive microwave measurements over crop fields. Remote Sens Environ 1995;51:331–41.
[135] Wigneron JP, Schmugge T, Chanzy A, Calvet JC, Kerr Y. Use of passive microwave remote sensing to moritor soil monitor. Agronomie 1998;18:27–43.
[136] Wigneron J-P, Waldteufel P, Chanzy A, Calvet J-C, Kerr Y. Two-D microwave interferometer retrieval capabilities of over land surfaces (SMOS Mission). Remote Sens Environ 2000;73(3): 270–82.
[137] Wilheit TT. Radiative transfer in a plane stratified dielectric. IEEE Trans Geosci Remote Sens 1978;GE-16:138–43.
[138] Yamaguchi Y, Kahle AB, Tsu H, Kawakami T, Pniel M. Overview of advanced spaceborne thermal emission and reflection radiometer (ASTER). IEEE Trans Geosci Remote Sens 1998;36:1062–71.
[139] Zobeck TM, Onstad CA. Tillage and rainfall effects on random roughness: a review. Soil Tillage Res 1987;9:1–20.